Design of an integrated coupler for the electrical generation of surface plasmon polaritons

J.-P. Tetienne,[1] A. Bousseksou,[1] D. Costantini,[1] Y. De Wilde,[2] and R. Colombelli[1,*]

[1]*Institut d'Electronique Fondamentale, Université Paris Sud and CNRS, UMR8622, 91405 Orsay, France*
[2]*Institut Langevin, ESPCI ParisTech, CNRS, 10 rue Vauquelin 75231 Paris Cedex 05, France*
**raffaele.colombelli@u-psud.fr*

Abstract: Recently a surface plasmon polariton (SPP) source based on an electrically operated semiconductor laser has been demonstrated. Here we present a numerical investigation of the light-SPP coupling process involved in the device. The problem consists in the coupling *via* a diffraction grating between a dielectric waveguide mode – the laser mode – and a SPP mode. The issue of the coupling efficiency is discussed, and the dependence on various geometrical parameters of both the grating and the dielectric waveguide is studied in detail. A maximum coupling efficiency of ≈24% is obtained at telecom wavelengths, which could lead to a high-power integrated SPP source when combined to a laser medium.

OCIS codes: (250.5403) Plasmonics; (140.5960) Semiconductor lasers.

References and links

1. S. A. Maier, *Plasmonics: Fundamentals and Applications* (Springer, 2007).
2. T. W. Ebbesen, C. Genet, and S. I. Bozhevolnyi, "Surface plasmon circuitry," Phys. Today **61**(5), 44–50 (2008).
3. W. L. Barnes, A. Dereux, and T. W. Ebbesen, "Surface plasmon subwavelength optics," Nature **424**(6950), 824–830 (2003).
4. S. Lal, S. Link, and N. J. Halas, "Nano-optics from sensing to waveguiding," Nat. Photonics **1**(11), 641–648 (2007).
5. E. Ozbay, "Plasmonics: merging photonics and electronics at nanoscale dimensions," Science **311**(5758), 189–193 (2006).
6. K. Kneipp, Y. Wang, H. Kneipp, L. T. Perelman, I. Itzkan, R. R. Dasari, and M. S. Feld, "Single molecule detection using surface-enhanced Raman scattering (SERS)," Phys. Rev. Lett. **78**(9), 1667–1670 (1997).
7. S. M. Nie and S. R. Emory, "Probing single molecules and single nanoparticles by surface-enhanced Raman scattering," Science **275**(5303), 1102–1106 (1997).
8. I. P. Radko, S. I. Bozhevolnyi, G. Brucoli, L. Martin-Moreno, F. J. Garcia-Vidal, and A. Boltasseva, "Efficiency of local surface plasmon polariton excitation on ridges," Phys. Rev. B **78**(11), 115115 (2008).
9. B. Hecht, H. Bielefeldt, L. Novotny, Y. Inouye, and D. W. Pohl, "Local excitation, scattering, and interference of surface plasmons," Phys. Rev. Lett. **77**(9), 1889–1892 (1996).
10. G. I. Stegeman, R. F. Wallis, and A. A. Maradudin, "Excitation of surface polaritons by end-fire coupling," Opt. Lett. **8**(7), 386–388 (1983).
11. H. Ditlbacher, N. Galler, D. M. Koller, A. Hohenau, A. Leitner, F. R. Aussenegg, and J. R. Krenn, "Coupling dielectric waveguide modes to surface plasmon polaritons," Opt. Express **16**(14), 10455–10464 (2008).
12. S. Y. Park, J. T. Kim, J. S. Shin, and S. Y. Shin, "Hybrid vertical directional coupling between a long range surface plasmon polariton waveguide and a dielectric waveguide," Opt. Commun. **282**(23), 4513–4517 (2009).
13. C. S. Kim, I. Vurgaftman, R. A. Flynn, M. Kim, J. R. Lindle, W. W. Bewley, K. Bussmann, J. R. Meyer, and J. P. Long, "An integrated surface-plasmon source," Opt. Express **18**(10), 10609–10615 (2010).
14. A. Babuty, A. Bousseksou, J.-P. Tetienne, I. M. Doyen, C. Sirtori, G. Beaudoin, I. Sagnes, Y. De Wilde, and R. Colombelli, "Semiconductor surface plasmon sources," Phys. Rev. Lett. **104**(22), 226806 (2010).
15. J. Decobert, N. Lagay, C. Cuisin, B. Dagens, B. Thedrez, and F. Laruelle, "MOVPE growth of AlGaInAs–InP highly tensile-strained MQWs for 1.3μm low-threshold lasers," J. Cryst. Growth **272**(1-4), 543–548 (2004).
16. V. Moreau, M. Bahriz, R. Colombelli, R. Perahia, O. Painter, L. R. Wilson, and A. B. Krysa, "Demonstration of air-guided quantum cascade lasers without top claddings," Opt. Express **15**(22), 14861–14869 (2007).
17. A. Bousseksou, Y. Chassagneux, J. R. Coudevylle, R. Colombelli, C. Sirtori, G. Patriarche, G. Beaudoin, and I. Sagnes, "Surface-plasmon distributed-feedback quantum cascade lasers operating pulsed, room temperature," Appl. Phys. Lett. **95**(9), 091105 (2009).
18. E. D. Palik, *Handbook of Optical Constants of Solids, Part II(1)* (Academic Press, 1985).
19. The commercial software package COMSOL Multiphysics was employed.

#150935 - $15.00 USD Received 12 Jul 2011; accepted 12 Aug 2011; published 31 Aug 2011

20. S. L. Chuang, *Physics of Optoelectronic Devices* (Wiley-Interscience, 1995).
21. P. Lalanne, J. P. Hugonin, H. T. Liu, and B. Wang, "A microscopic view of the electromagnetic properties of sub-λ metallic surfaces," Surf. Sci. Rep. **64**(10), 453–469 (2009).

1. Introduction

Surface plasmon polaritons (SPPs) are electromagnetic modes confined to the close vicinity of a metal-dielectric interface, which originate from charge density oscillations coupled to the photon field [1]. Recent interest in plasmonics is motivated in part by two possible applications: integrated plasmonics [2,3] and nanosensing [4]. The former one is expected to provide a technology capable of transmitting signals at the sub-micron-scale and with optical data-rates, thus bridging fast – but diffraction limited – photonics and highly integrated – but strongly speed limited by the RC delay – electronics [5]. The latter application, i.e. sensing, relies on surface plasmon resonances whose frequency is shifted by the presence of a substance/analyte. Alternatively, the huge field enhancements in properly designed plasmonic structures can be exploited to increase otherwise very weak Raman signals [6,7].

However, a fundamental issue in plasmonics which is still not completely solved is how to efficiently generate and launch SPPs into plasmonic waveguides. This task is generally achieved by coupling light from free space or from conventional optical waveguides into plasmonic structures through momentum matching (prism coupling [1], grating coupling [8], nanoparticle scattering [9]), end-fire coupling [10,11], or mutual directional coupling [12]. However, an integrated source capable of generating SPPs under electrical injection would be a crucial step towards miniaturization for both applications [13].

Recently a semiconductor surface plasmon polariton source has been experimentally demonstrated [14] at mid-infrared wavelengths. It is comprised of an electrically pumped laser cavity topped by a passive plasmonic waveguide into which SPPs are launched thanks to a grating coupler. The role of the coupler, which is in fact a metallic grating, is to compensate the momentum difference between the laser mode and the SPP wave. Hence the device in [14] is able to couple a SPP beam into a passive waveguide under electrical injection, paving the way for integrated plasmonic circuitry and miniaturization of plasmon-based sensors. The general scheme of the device is shown in Fig. 1. Besides its use as an integrated SPP source when combined with a laser medium, the technique can be employed as a passive coupling scheme to convert guided photons into SPPs. Compared to other configurations, such a coupler is compact [12] and it can be easily integrated [11] since it is sufficient to just deposit a metallic layer – comprised of the SPP-carrying strip and the diffraction grating – above the dielectric waveguide layers.

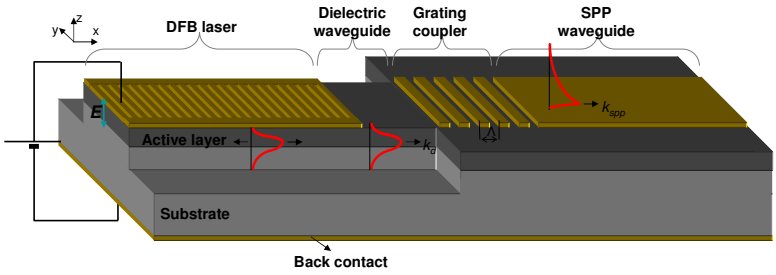

Fig. 1. Scheme of the SPP source. The device comprises an active section – a distributed feedback laser – and a passivecoupler designed to inject SPPs into a metal-air interface mode.

In this paper we investigate the efficiency of the grating coupler which permits the SPP generation. Numerical simulations relying on a finite-element approach are performed, and we find a maximum coupling efficiency higher than 24%. Although the concept has been experimentally demonstrated at mid-infrared wavelengths (λ≈8 μm) [14], we choose here to carry out the study at telecom wavelengths (especially at λ≈1.3 μm). Not only the tighter

#150935 - $15.00 USD Received 12 Jul 2011; accepted 12 Aug 2011; published 31 Aug 2011

spatial confinement of SPPs at short wavelengths eases the numerical modeling of the problem, but especially the results can be directly applied to implement an efficient SPP source that operates at telecom wavelengths, a device which would be of much interest for the field of plasmonics.

2. Calculation setup

2.1 Structure details

We consider a dielectric waveguide composed of a high-index core (index n_c, thickness t_c) sandwiched between two semi-infinite lower-index media, a substrate (index n_s) at the bottom and air (n_a = 1) at the top (see Fig. 2). The metallic layer (index n_m, thickness t_m) is located above the waveguide core and it comprises both the SPP-carrying film and the grating coupler. Figure 2 defines the coordinate system and the resulting geometry, which is assumed to be infinite along the y-direction. The grating is characterized by its period Λ, its duty cycle dc = d/Λ where d is the width of the metallic fingers, and the number of periods N. Its role is to provide the missing momentum between guided photons and SPPs. An efficient coupling is expected provided that the x-component of the wave-vector – k_d and k_{spp} – of the dielectric waveguide mode and of the SPP wave (see Fig. 2), respectively, satisfy the phase-matching condition:

$$k_d = k_{spp} + p \cdot \frac{2\pi}{\Lambda}, \tag{1}$$

where p is an integer. For first order diffraction p = 1, the period Λ is then given by:

$$\Lambda = \frac{\lambda_0}{n_d - n_{spp}}, \tag{2}$$

where n_d and n_{spp} denote the effective indices of the dielectric waveguide mode and the SPP mode, respectively, and λ_0 is the free space wavelength. Because of the transverse magnetic (TM) polarization of SPPs, we only consider the fundamental TM mode of the dielectric waveguide. The refractive indices of the dielectric layers used in the following (n_c = 3.45 and n_s = 3.2) are typical average values for AlGaInAs tensile-strained multiple-quantum wells (MQWs) grown on an InP substrate. Such structures are known to exhibit elevated TM modal gains and they are employed to realize TM-polarized lasers emitting at λ≈1.3 μm [15]. We highlight the fact that, although conventional lasers usually comprise an upper cladding, laser structures whose active layer is directly covered by the electrical top contact or even by air have been demonstrated [16,17]. We study this geometry in this paper since it is advantageous in order to achieve larger coupling efficiencies into the SPP mode. The frequency-dependent complex refraction index for gold will be taken from [18].

#150935 - $15.00 USD Received 12 Jul 2011; accepted 12 Aug 2011; published 31 Aug 2011

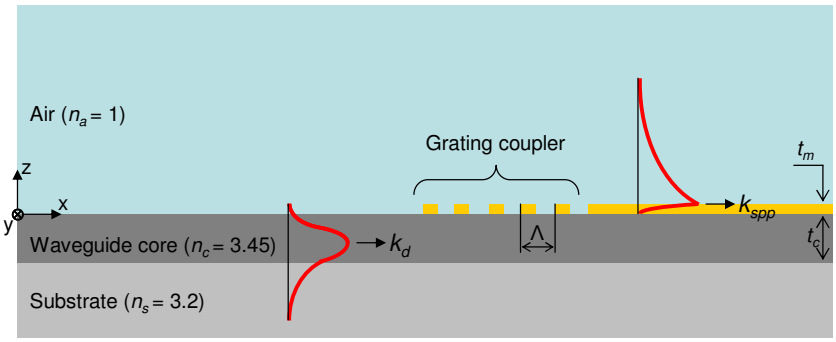

Fig. 2. Geometry of the configuration under study. The structure is assumed to be infinite in the y-direction. The frequency-dependent gold index nm is taken from [18]. The red curves represent the typical mode profiles of the two modes to be coupled.

2.2 Numerical calculation details

All numerical results were obtained by performing systematic two-dimensional (2D) simulations using a finite-element method [19]. The simulation strategy consists in injecting the fundamental TM mode – at a wavelength λ_0 – from the left waveguide boundary [20], while all the other boundaries feature absorbing conditions. The coupling efficiency is defined as the ratio

$$\eta = \frac{P_{spp}}{P_d}, \tag{3}$$

where P_{spp} and P_d are the electromagnetic power fluxes carried by the SPP mode and by the forward propagating dielectric waveguide mode, respectively.

In order to link these two quantities to the magnetic field distribution that will be numerically calculated, we first recall the basic formulae for a slab waveguide [20]. The TM_0 mode of the **asymmetric dielectric slab** waveguide is fully characterized by its magnetic vector field $\mathbf{H}(\mathbf{r},t) = H_y(x,z)e^{i\omega t}\mathbf{e}_y$. The spatial distribution $H_y(x,z)$ can be written as follows:

$$H_y(x,z) = H_{\max}^d e^{-ik_d x} \begin{cases} \cos(\varphi)e^{-\alpha_a z} & for \;\; z > 0 \\ \cos(k_z z + \varphi) & for \;\; -t_c < z < 0 \\ \cos(-k_z d + \varphi)e^{-\alpha_s (z+t_c)} & for \;\; z < -t_c \end{cases}, \tag{4}$$

where the constants k_d, α_a, α_s and k_z must satisfy the relations:

$$\begin{cases} k_z d = \tan^{-1}\left(\frac{\varepsilon_c \alpha_a}{\varepsilon_a k_z}\right) + \tan^{-1}\left(\frac{\varepsilon_c \alpha_s}{\varepsilon_s k_z}\right) \\ \varepsilon_a k_0^2 = k_d^2 - \alpha_a^2 \\ \varepsilon_c k_0^2 = k_d^2 + k_z^2 \\ \varepsilon_s k_0^2 = k_d^2 - \alpha_s^2 \end{cases}, \tag{5}$$

with $\varphi = \tan^{-1}\left(\varepsilon_c \alpha_a / \varepsilon_a k_z\right)$ and $\varepsilon_i = n_i^2$ are the dielectric constants. The power flux can be obtained by taking the *real* part of the complex Poynting vector and integrating over z:

#150935 - $15.00 USD Received 12 Jul 2011; accepted 12 Aug 2011; published 31 Aug 2011

$$P_d = \int dz \frac{1}{2} \mathrm{Re}\left\{(\mathbf{E}\times\mathbf{H}^*)\cdot\mathbf{e}_x\right\} = \left|H^d_{\max}\right|^2 \frac{k_d}{4\omega\varepsilon_0}\left[\frac{\cos^2(\varphi)}{\varepsilon_a\alpha_a}+\frac{d}{\varepsilon_c}+\frac{\sin(2\varphi)-\sin(-2k_z d+2\varphi)}{2\varepsilon_c k_z}+\frac{\cos^2(-k_z d+\varphi)}{\varepsilon_s\alpha_s}\right]. \quad (6)$$

Likewise, the **SPP mode at the metal-air interface** is fully characterized by its magnetic vector field $\mathbf{H}(\mathbf{r},t) = H_y(x,z)e^{i\omega t}\mathbf{e}_\mathbf{y}$. The spatial distribution $H_y(x,z)$ can be written as follows:

$$H_y(x,z) = H^{spp}_{\max} e^{-ik_{spp}x}\begin{cases} e^{-\alpha'_a(z-t_m)} & for\ \ z > t_m \\ e^{\alpha_m(z-t_m)} & for\ \ z < t_m \end{cases}, \quad (7)$$

where the constants k_{spp}, α'_a and α_m must satisfy the relations:

$$\begin{cases} k_{spp} = k_0\dfrac{\varepsilon_a\varepsilon_m}{\varepsilon_a+\varepsilon_m} \\ \varepsilon_a k_0^2 = k_{spp}^2 - \alpha'^2_a \\ \varepsilon_m k_0^2 = k_{spp}^2 - \alpha_m^2 \end{cases}. \quad (8)$$

The power flux is then related to $H^{spp}_{\max}$ *via* the following formula:

$$P_{spp} = \int dz \frac{1}{2}\mathrm{Re}\left\{(\mathbf{E}\times\mathbf{H}^*)\cdot\mathbf{e}_x\right\} = \left|H^{spp}_{\max}\right|^2 \mathrm{Re}\left\{\frac{k_{spp}}{4\omega\varepsilon_0}\left[\frac{1}{\varepsilon_a\,\mathrm{Re}\{\alpha'_a\}}+\frac{1}{\varepsilon_m\,\mathrm{Re}\{\alpha_m\}}\right]\right\}. \quad (9)$$

Back to the whole geometry of Fig. 2, we now explicit how P_d and P_{spp} are inferred from the numerically calculated magnetic field amplitudes. In Eq. (6), the unknown quantity $H^d_{\max}$ is evaluated from the maximum field in the core layer, namely $H^d_{\max} = \left\langle\left|H_y\left(x, z=-\varphi/k_z\right)\right|\right\rangle_x$. The symbol $\langle\cdot\rangle_x$ stands for the average value over one spatial period of the guided wave. Indeed, the grating coupler induces a reflected wave resulting in a partially standing wave in the dielectric waveguide. Since the boundary condition imposes the total amplitude at a given *x*, we don't know a priori the forward amplitude and therefore the average operation is required. Note that with this technique we are able in principle to readily determine the grating-induced reflection coefficient as well.

On the other hand, the unknown quantity $H^{spp}_{\max}$ in Eq. (9) is related to the field amplitude at the metal-air interface $\left|H_y\left(x=x_0, z=t_m\right)\right|$, x_0 being the left edge of the metallic film. However, in order for the total field at the metal-air interface to correspond to the sole SPP contribution, we need to monitor it at a distance x_e sufficiently far from the coupler, and then subtract the propagation loss of the SPPs as η is defined at the coupler location. Precisely, we use $H^{spp}_{\max} = \left|H_y\left(x=x_0+x_e, z=t_m\right)\right| / \exp\left(-\mathrm{Im}\left\{k_{spp}\right\}x_e\right)$, with x_e = 100 μm in all calculations, and k_{spp} is the SPP complex wave-vector as expressed in Eq. (8). This guarantees that the contribution of the radiating - non-guided - waves launched from the coupler together with the SPPs becomes negligible [21]. The power fluxes P_d and P_{spp} are then calculated with Eq. (6) and Eq. (9), respectively, which finally leads to the coupling efficiency η of Eq. (3).

#150935 - $15.00 USD Received 12 Jul 2011; accepted 12 Aug 2011; published 31 Aug 2011

3. Numerical results

3.1 Wavelength dependence of the coupling efficiency

First, we investigate the wavelength dependence of the SPP excitation efficiency. The Fig. 3(a) shows the calculated coupling efficiency for the wavelength range 1.15-1.5 μm. The waveguide core is 500 nm thick, the grating has a 50%-duty-cycle, a period of 570 nm, and the metal thickness is 100 nm. The number of periods is spanned from 2 to 20 (for clarity, data are plotted only for some values of N between 2 and 12). As expected from an interference-based coupling, a resonance wavelength appears as the number of periods is increased, while its frequency width narrows around a central value of $\lambda \approx 1.3$ μm. As shown in the inset of Fig. 3(a), the maximum SPP coupling efficiency steadily increases with N, and it reaches a maximum value of about 13% for N = 12. For larger values of N, the coupling efficiency saturates: the impinging guided wave is almost totally scattered - into SPPs, but also in the air and in the substrate - after roughly 12 periods, making the following periods redundant.

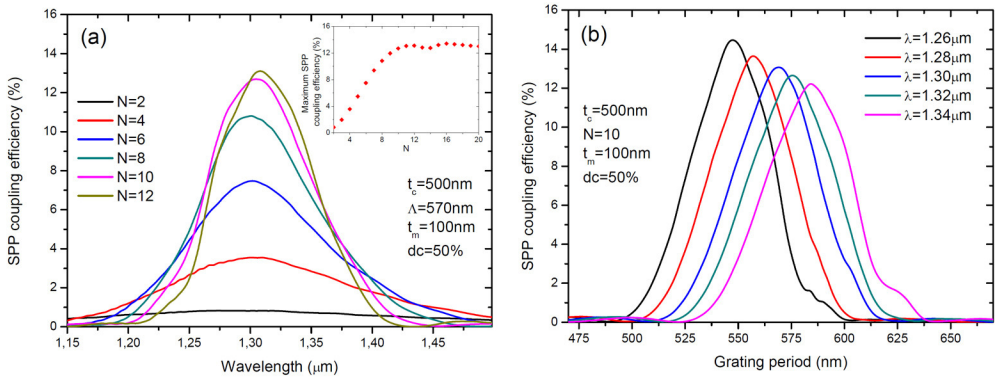

Fig. 3. (a) Calculated SPP coupling efficiency as a function of the wavelength. Different curves show data for various numbers N of periods composing the grating. Inset: Maximum SPP coupling efficiency versus N. (b) Calculated SPP coupling efficiency as a function of the grating period Λ for various wavelengths.

For all the following calculations, we used N = 10, which offers a good trade-off between efficiency and compactness: such a coupler is in fact shorter than 6 μm in length. Furthermore, this choice yields a relatively broadband device: $\Delta\lambda/\lambda \approx 10\%$, where $\Delta\lambda$ is the full-width at half-maximum (FWHM). This feature can be particularly useful in the context of telecommunications, if the coupler is employed as a passive photon-to-SPP converter.

In view of designing a SPP source based on a quasi-monochromatic laser, the issue of the period-sensitivity is of more practical importance. Figure 3(b) shows the SPP coupling efficiency as a function of the grating period Λ for various excitation wavelengths. From the plots, which exhibit a resonant behavior which roughly follows Eq. (2), a FWHM of about 50 nm is estimated. This value is sufficient to ensure some flexibility for fabrication with standard techniques based on electron-beam lithography. We also notice that the peak values for η in Fig. 3(b) are wavelength-dependent. This effect possibly stems from the index dispersion of gold, since it disappears when the calculations are performed with a non dispersive dielectric function (data not shown). The intuitive physical reason is that the SPP mode is more extended in the dielectric at larger wavelengths, hence the SPP excitation via a localized source near the metal-dielectric interface - that is, our coupler – is less efficient. An analogous effect has been rigorously demonstrated in the case of a single slit in a metallic film illuminated at normal incidence [21].

#150935 - $15.00 USD Received 12 Jul 2011; accepted 12 Aug 2011; published 31 Aug 2011

3.2 Dependence on the geometrical parameters

In this section, we show that it is possible to further increase the maximum coupling efficiency η by fine tuning the geometrical parameters of the grating coupler, namely its thickness and duty cycle. The period Λ is kept fixed. We have performed numerical simulations of SPP excitation and coupling efficiency with a grating whose duty cycle is varied from 0% to 100%, and the metal thickness spans the 50-250 nm range (see Fig. 4). The number of periods (N = 10) and the waveguide core thickness (t_c = 500 nm) are kept constant. The wavelength used for the calculations is λ = 1.3 μm while the data are shown for various grating periods.

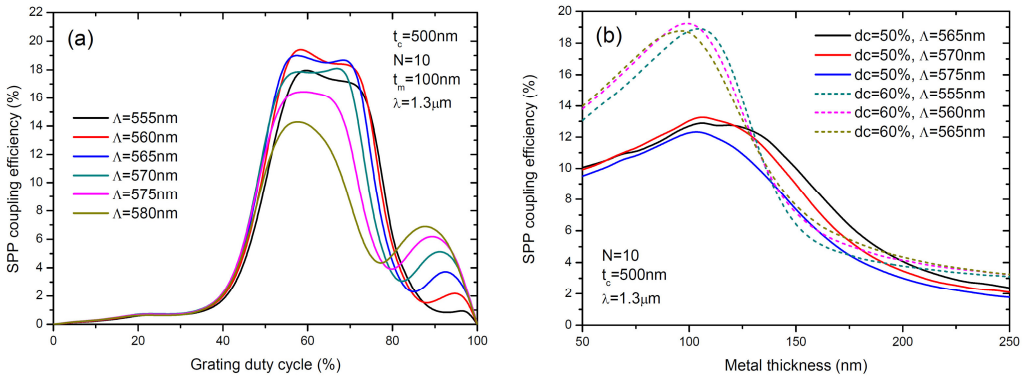

Fig. 4. Calculated SPP coupling efficiency as a function of the grating duty cycle dc (a), and the metal thickness t_m (b) for various grating periods Λ. The data in panel (b) are shown for both dc = 50% and dc = 60%.

Figure 4(a) shows that the largest SPP coupling efficiencies of ≈20% are obtained for duty cycles between 60% and 70%. It also appears that the grating period yielding the highest value is Λ = 560 nm (60% duty cycle) while it is 570 nm for a 50% duty cycle. This is due to a small variation of the effective index undergone by the impinging guided wave when it propagates under the grating. Hence, the coupling condition Eq. (2) depends on the grating shape *via* the effective index modulation. This effect is visible in Fig. 4(b) as well, since the optimal period Λ depends on the grating thickness. In any case, Fig. 4(b) confirms that the very reasonable value of 100 nm for the metal thickness is a good choice.

3.3 Dependence on the input waveguide thickness

In view of designing a SPP source, it is important to assess its sensitivity with respect to the input dielectric waveguide dimensions. Especially, the waveguide core thickness should be imposed by the laser technology employed. Figure 5 shows the SPP excitation efficiency calculated at λ_0 = 1.3 μm for a 10-period grating with t_m = 100 nm. Various grating periods as well as two different duty cycles are investigated. The dielectric waveguide core thickness is varied between 250 nm, which roughly corresponds to the cut-off thickness for the fundamental TM mode, and 750 nm.

#150935 - $15.00 USD Received 12 Jul 2011; accepted 12 Aug 2011; published 31 Aug 2011

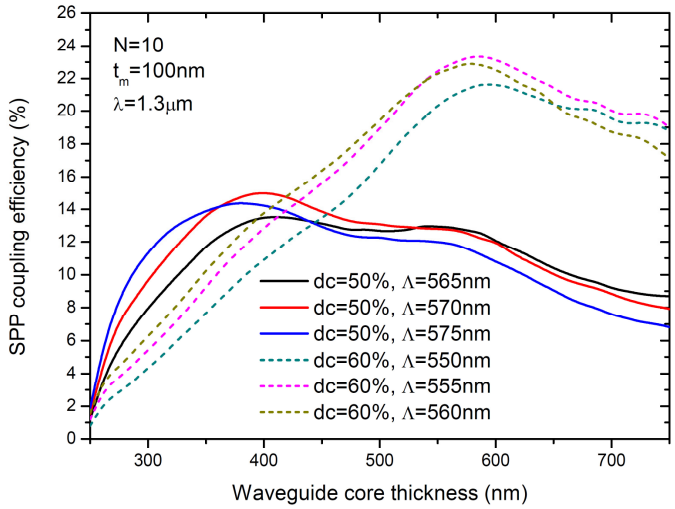

Fig. 5. Calculated SPP coupling efficiency as a function of the waveguide core thickness t_c for various grating periods Λ and for both dc = 50% and dc = 60%.

Since the coupling mechanism relies on the coherent scattering of the impinging guided wave, the SPP excitation efficiency should strongly depend on how this wave interacts with the grating. In particular, we expect the extreme cases to be unfavorable. Near the cut-off thickness (t_c≈250 nm) the mode penetrates excessively into the substrate, while for large values of t_c it is more and more confined in the waveguide core. Hence in both cases the field at the core-air interface is comparatively very weak.

The duty cycle too plays a role in this interaction. We find a maximum η of ≈15% for a 400-nm-thick core layer with Λ = 570 nm and dc = 50%, while with dc = 60%, Λ = 555 nm and t_c = 600 nm, the coupling efficiency jumps to 24%. The situation is well illustrated in Fig. 4, which highlights the importance of optimizing all parameters *simultaneously* in order to optimize the coupler. Note that increasing N can further improve the efficiency of a few percents, but to the detriment of a reduced compactness.

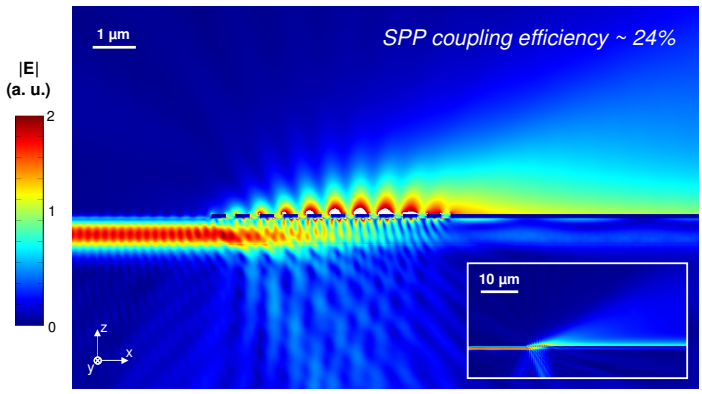

Fig. 6. Electric field distribution calculated for the problem described in Fig. 2 with the optimized parameters t_c = 600 nm, N = 10, Λ = 555 nm, dc = 60%, t_m = 100 nm. The wavelength of the impinging guided wave is λ_0 = 1.3 μm. The data are plotted in linear color scale with an arbitrary unit. Inset: overall view of the simulated area.

We conclude this section by plotting the electric field distribution calculated at λ_0 = 1.3 μm with the aforementioned set of optimized parameters (Fig. 6). The SPP wave launched at the metal-air interface is clearly distinguishable, as well as the light scattered in the substrate

#150935 - $15.00 USD Received 12 Jul 2011; accepted 12 Aug 2011; published 31 Aug 2011

and in the air. Our calculations in Fig. 4 showed that ≈24% of the power propagating in the input waveguide is coupled into the SPP mode. Hence, if this coupler was combined to a semiconductor laser, as in Fig. 2, it could potentially lead to a compact injection device capable of generating a coherent, directional and powerful SPP beams.

4. Conclusions

We have numerically demonstrated an integrated coupler capable of injecting up to 24% of the power carried by a dielectric waveguide mode into a SPP wave at an air-metal interface. The device operates at telecom wavelengths. We showed that a good coupling efficiency is obtained with a reasonably large range of geometrical parameters. Such flexibility is also observed in terms of input wavelength: the coupler operation is relatively broadband. This study confirms the potential of a concept which has been initially investigated in the mid-infrared [14], but could lead to the demonstration of an efficient electrically injected SPP semiconductor source at telecom wavelengths. More generally, this coupling technique could be useful to implement optoelectronic devices capable of generating, amplifying or detecting SPPs [13].

Acknowledgments

We acknowledge financial support from the French National Research Agency (ANR-09-NANO-020 “Gospel”).

#150935 - $15.00 USD Received 12 Jul 2011; accepted 12 Aug 2011; published 31 Aug 2011